Behavior of normal-strength recycled aggregate concrete filled steel tubes under combined loading

Jie Chen [a,b], Yuyin Wang [a,*], Charles W. Roeder [c], Ji Ma [d]

[a] Key Lab of Structures Dynamic Behavior and Control of the Ministry of Education (Harbin Institute of Technology), Harbin 150090, China
[b] Shenzhen Graduate School, Harbin Institute of Technology, Shenzhen 518055, China
[c] Civil & Environmental Engineering, University of Washington, Seattle, WA 98195-2700, USA
[d] Ministry of Housing and Urban-Rural Development of the People's Republic of China (MOHURD), Beijing 100835, China

ARTICLE INFO

ABSTRACT

The use of recycled aggregate concrete (RAC) for the fill in concrete filled steel tube (CFST) members (RACFST members) is proposed as a practical structural application. An experimental study of RACFST members with normal-strength concrete under combined loading is summarized. Forty-eight columns and three beams in groups of 3 identical specimens were tested to failure. Study parameters included recycled coarse aggregate (RCA) replacement percentage, source of RCA, eccentricity, slenderness, and the steel to concrete area ratio. Experimental results are consistent with less than 3% scatter within each group. The maximum compressive load of the columns decreased modestly with increasing substitution level of RCA (up to 11.2%), and the structural effects of the recycled aggregate replacement on load capacity and initial stiffness are smaller than the corresponding changes in material properties. The source of RCA had little effect on the behavior of RACFST under combined loading for this test program, and the similar size grading and index of crushing obtained in the aggregates may have provided this benefit. These observations support the use of RACFST in structural engineering. Current CFST design provisions are compared to the RACFST test results, and the design recommendations for RACFSTs are presented.

© 2016 Elsevier Ltd. All rights reserved.

1. Introduction

The use of construction and demolition waste as alternative aggregates for new concrete production preserves natural sources and reduces the waste disposal requirements [1,2]. Unfortunately, reuse of demolished concrete has been limited to pavement base, backfill for retaining walls, and other uses that do not require high structural performance [3], due to the low strength, high short- and long-term deformations, and large scatter of the compressive strength in the test results for recycled aggregate concrete (RAC) [4–7].

Concrete filled steel tubes (CFST) are composite structural members that consist of a steel tube and concrete infill, which have been widely used in civil engineering practice as columns, bridge piers, and caissons due to the combined advantages of the steel tube and the concrete core [8–13]. The use of RAC as the concrete fill of CFST is proposed as a practical structural application of RAC. The steel tube provides a restraining action to the transverse expansion of the RAC infill, thereby offering enhanced load bearing

capacity and ductility. Further, the steel tube seals the concrete fill and this benefits the durability of RAC infill [14–17]. The contribution of outer steel tube may also reduce the scatter of the mechanical properties of the RAC core.

To date, researchers have mostly focused on the axial response of circular recycled aggregate concrete filled steel tubular (RACFST) stub columns [18–23], while limited attention has been devoted to their combined axial-flexural response. Yang and Han [24] reported one of the earliest experimental studies on the slender columns of circular RACFST under axial and eccentric loading. Their research considered recycled coarse aggregate (RCA) replacement percentages, r, of 0%, 25% and 50%, slenderness ratio, λ ($\lambda = 4L/D$), of 40 and the steel to concrete area ratio, α ($\alpha = A_s/A_c$), of 6%. Chen et al. [25,26] examined the behavior of eccentrically loaded circular RACFST slender columns with α ratio of 11% and wider RCA replacement ratios ranging from 0% to 100%. The influence of the eccentricity ratio, e/r_0 (e is eccentricity of load and $r_0 = D/2$), on the behavior of RACFST specimens has also been considered [24–26]. Yang and Han [18] conducted experiments on the flexural behavior of 4 circular RACFSTs with RCA replacement ratios between 0% and 50%.

---

* Corresponding author.
  E-mail address: wangyuyin@hit.edu.cn (Y. Wang).

Nomenclature

CFST	concrete filled steel tube
NCA	natural coarse aggregate
RAC	recycled aggregate concrete
RACFST	recycled aggregate concrete filled steel tube
RCA	recycled coarse aggregate
RCA-L	recycled coarse aggregate from laboratory waste concrete
RCA-P	recycled coarse aggregate from real building demolition project
SSD	saturated-surface-dry condition for recycled coarse aggregates
A	cross-sectional area of column
A_c	cross-sectional area of concrete core
A_s	cross-sectional area of steel tube
D	external diameter of steel tube
DI	ductility index
e	eccentricity
e/r_0	eccentricity ratio
EA	elastic stiffness of columns
$E_{c,28}$	Young's modulus of concrete at 28 days
$E_{c,test}$	Young's modulus of concrete at test days
E_s	Young's modulus of steel tube
$f_{cm,28}$	concrete cylinder strength at 28 days
$f_{cm,test}$	concrete cylinder strength at test days
$f_{cu,28}$	concrete cubic strength at 28 days

$f_{cu,test}$	concrete cubic strength at test days
f_u	ultimate tensile strength of steel tube
f_y	yield strength of steel
L	length of columns
M	moment resisted by columns during the tests
P	axial load resisted by columns during the tests
P_{ce}	axial load resisted by columns corresponding to the onset of confinement effects
P_u	experimental maximum compressive load of columns
r	replacement ratio of RCA
r_0	radius of cross section, $r_0 = D/2$
t	wall thickness of steel tube
w/c	water-cement ratio
u_m	mid-span deflection at maximum compressive load
α	steel to concrete area ratio, $\alpha = A_s/A_c$
$\varepsilon_{s,c}$	circumferential strain of steel tube
$\varepsilon_{s,v}$	vertical strain of steel tube
ε_v	vertical axial strain of columns
μ_s	poisson's ratio of steel tube
μ_{steel}	ratio of horizontal deformation over vertical deformation for steel in coupon tests
$\triangle_u$	vertical displacement at maximum compressive load
$\triangle_{0.85}$	vertical displacement at $0.85P_u$ after maximum compressive load

---

The previous studies investigated the effect of the substitution level of RAC for normal aggregate concrete on the behavior of circular RACFST members with particular α ratios and sources of the RCA. However, there is no reported research relevant to the influence of the α ratio and RCA source on the response of RACFST composite members under combined loading. The flexural behavior of RACFST beams with 100% replacement is also not studied. Although the mechanical behavior of RAC has been extensively investigated, the use of RAC in structural application may still be questioned by engineers due to the large scatter in the material test results. Twelve prior circular RACFST slender columns were tested to failure to investigate their static response to axial and eccentric loads, but this is not enough to verify and establish design equations for RACFST columns subjected to various loading conditions.

This study provides a comprehensive experimental study for RACFST members with normal-strength concrete under combined loading, and it develops and expands the experimental database and benchmark data for the development of design recommendations for RACFST members. Forty-eight columns and three beams were tested to failure. These tests were designed to investigate the effects of RCA replacement ratio (r), the steel to concrete area ratio (α), the slenderness ratio (λ), the eccentricity ratio (e/r_0) and the source of RCA on the response of specimens. In addition, the scatter in the measured performance of RACFSTs under combined loading was analyzed. Finally, the reliability of current CFST design provisions for predicting the behavior of RACFSTs under combined loading is evaluated using these test results as well as data from prior studies.

2. Experimental study

2.1. Design of RACFST specimens

Current design codes, such as EC4 (EN 1994-1-1 [27]) in Europe, AISC (AISC 360-10 [28]) in US, and GB (GB50936-2013 [29]) in China, provide methods to estimate and evaluate CFST behavior, but they are not yet verified for RACFSTs. In designing RACFST specimens for this study, the axial load-moment strength (P-M) interaction curves of CFSTs are initially analyzed using the EC4 method [27]. The parameters of slenderness ratio, λ = 12, 32 and 48, and the eccentricity, e, are considered in this analysis, and the results of the EC4 evaluation are presented in Fig. 1.

The diameter and the thickness of the tube are 140 mm and 2.75 mm, respectively, the steel to concrete area ratio, α, is 8%, and the cylinder strength of the concrete core and yield stress of steel tube are 35 MPa and 310 MPa, respectively. The RCA replacement ratio, source of RCA, α ratio, and eccentricity are variables in the design of the RACFST specimens. RCA replacement ratios of 0%, 50% and 100% were used for the specimens with slenderness ratio of 32 and eccentricities of 20 mm and 40 mm (e/r_0 = 0, 0.29 and 0.58, triangle shape points in Fig. 1). Two sources of RCA are used for the specimens with slenderness ratios of 12 and 32 under axial loading (circle shape points in Fig. 1). One source of the RCA was derived from 2-year-old laboratory concrete with concrete proper-
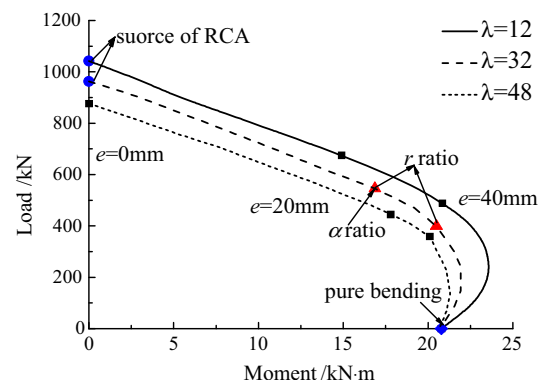

Fig. 1. Design of RACFST specimens.

ties consisting of a water-cement ratio of 0.46 and a cubic compressive strength of about 49 MPa. The other source was derived from demolition of a 15-year-old three-story building in Harbin with concrete properties consisting of a water-cement ratio of 0.45 and a cubic compressive strength of about 40 MPa. The α ratios of 8%, 11% and 14% are used for the specimens with slenderness ratio of 32 and eccentricity of 20 mm (triangle shape point at $e = 20$ mm in Fig. 1). In order to determine the axial load-moment strength (P-M) interaction curves for RACFSTs, the beam specimen with 100% replacement is also included in the design (diamond shape point at $y = 0$ axis in Fig. 1).

A total of 48 circular RACFST columns and 3 beams were tested with 17 groups of 3 identical specimens. Details of the specimens are shown in Table 1. In addition, a group of stub columns filled with aggregate from building demolition project tested by the authors [23] (Group 2 in Table 1) were used in the comparison with the test results in this study. An example of the test specimen identification system is as follows: CL12-8-100-0, where CL represents a composite column with the aggregate from the laboratory (CP depicts a composite specimen with aggregate from the building demolition project), the next digit number '12' is the nominal slenderness ratio ($\lambda = 4L/D$), the following digit '8' accounts for the nominal α ratio of 8%, the next one '100' denotes the RCA replacement ratio of 100%, the digit '0' defines eccentricity of load with 0 mm (∞ defines the specimen under flexural loading with infinite eccentricity), and the letters 'a, b, c' are used to identify the 3 identical specimens in each specimen group.

2.2. Material properties

The quality control of recycled aggregates in terms of the size grading and basic physical properties is very important for the preparation of RAC, since aggregates play a fundamental role in determining workability, strength and durability of concrete [6]. The specification from RILEM (RILEM TC 121-DRG) [30] classifies three categories for RCAs and the type II and type III RCAs are recommended to be applied for structural concrete. (Appendix A). The requirements on the properties for type III RCA are relatively higher. However, the maximum allowable replacement ratio of type III RCA for concrete is only 20%. The focus of this study is to show the structural application of RAC in CFSTs. The behavior of RAC core should be improved due to the existence of the outer steel tube and the confinement effects. Thus, the replacement ratio

of RCA for RACFSTs is supposed to be higher. According to the specification, there is no limit on the replacement ratio of type II RCA and this type of aggregate is allowed to be used for concrete with maximum strength class of C50/60. These are in accordance with the focus of this study. Therefore, the qualities of the RCA used in this study were controlled to meet the requirements of type II RCA in RILEM TC 121-DRG. The requirements for structural concrete using RCA in RILEM TC 121-DRG are also consistent with those in code DAfStb of Germany for RAC [31].

Two RCAs and one natural coarse aggregate (NCA) were used in this research. The original virgin aggregate of RCAs was granite stone that was similar to the NCA. The concrete wastes were crushed and assorted properly to create size grading similar to NCA with the goal of obtain required workability and strength for RAC used in CFSTs. The size grading analysis was carried out in accordance with Chinese code JGJ 52-2006 [32]. The test results are summarized in Table 2, which meet the requirements in JGJ 52-2006 [32] for crushed stone.

The RCA is similar in appearance to the NCA although. However, its texture is rougher and its shape is more irregular due to adhered mortar. The physical properties of these aggregates summarized in Table 2 shows that the notable distinctive features of RCAs compared with natural aggregate are their lower density and higher absorption capacity, mainly due to the adhered mortar and the high amount of cracks caused by crushing process. According to the test results, the RCAs in this study meet the requirements for type II RCA in RILEM TC 121-DRG [30].

The concrete mix with an effective water-cement ratio of 0.45 adopted for the RACFST specimens is outlined in Table 3. The mixes are designed for the concretes with cylinder strength of 35 MPa at 28 days. The irregular shape and high absorption capacity of recycled aggregates have adverse effects on the properties of fresh and harden concrete, particularly its consistency and strength [5,33–35]. Thus, the recycled aggregate was pre-wetted or pre-soaked before concrete mixing in order to obtain workability and mechanical properties required of the concrete [4,36–39]. Additionally, the wet processing technique for RCA can provide better quality aggregate with less organic and inorganic impurities and the adverse effect of RCA can therefore be minimized [40]. Details regarding the production of RAC can be found in the reported work by the authors [23]. The workability of the concretes is also listed in Table 3. A slump reduction has been observed for RAC in the tests, mainly due to the heterogeneity and rough texture of the recycled

Table 1
Details of test specimens.

Loading type	Group	Specimen labels	D (mm)	t (mm)	L (mm)	α (%)	λ	r (%)	e (mm)	e/r_0
Axial loading	1	CL12-8-100-0	137.91	2.70	420	8.4	12	100	0	0
	2	CP12-8-100-0[23]	137.67	2.72	420	8.4	12	100	0	0
	3	CL32-8-100-0	137.73	2.69	1120	8.3	32	100	0	0
	4	CP32-8-100-0	137.63	2.72	1120	8.4	32	100	0	0
	5	CL48-8-100-0	137.76	2.73	1680	8.4	48	100	0	0
Eccentric loading	6	CL12-8-100-20	137.70	2.71	420	8.4	12	100	20	0.29
	7	CL12-8-100-40	137.59	2.71	420	8.4	12	100	40	0.57
	8	CL32-8-100-20	137.52	2.73	1120	8.4	32	100	20	0.29
	9	CL32-11-100-20	140.20	3.52	1120	10.8	32	100	20	0.29
	10	CL32-14-100-20	141.64	4.30	1120	13.3	32	100	20	0.29
	11	CL32-8-50-20	137.75	2.72	1120	8.4	32	50	20	0.29
	12	CL32-8-0-20	137.66	2.72	1120	8.4	32	0	20	0.29
	13	CL32-8-100-40	137.38	2.70	1120	8.3	32	100	40	0.57
	14	CL32-8-50-40	137.75	2.70	1120	8.3	32	50	40	0.57
	15	CL32-8-0-40	137.69	2.73	1120	8.4	32	0	40	0.57
	16	CL48-8-100-20	137.82	2.71	1680	8.4	48	100	20	0.29
	17	CL48-8-100-40	137.75	2.74	1680	8.5	48	100	40	0.57
Pure bending	18	CL36-8-100-∞	137,73	2.70	1260	8.3	36	100	∞	∞

Note: Three identical specimens are designed in each group.

Table 2
Basic properties of natural coarse aggregate and recycled coarse aggregates.

Type	Grading (mm)	Cumulative passing by weight (%)				Density (kg/m^3)	Water absorption (%)	Index of crushing (%)	Residual mortar content (%)
		26.5 mm	16.0 mm	4.75 mm	2.36 mm				
NCA	4.75-25	100	55.0	1.6	0	2880	0.57	3.1	–
RCA-L	4.75-25	100	62.0	2.5	0	2660	7.46	9.7	48
RCA-P	4.75-25	100	65.0	2.0	0	2675	6.50	8.7	49

Note: NCA depicts the natural coarse aggregate; RCA-L and RCA-P represents the recycled coarse aggregate from laboratory waste concrete and building demolition project, respectively.

Table 3
Mix composition of concrete.

RCA resource	r (%)	Effective w/c	Materials (kg/m^3)					Slump (mm)
			Water (w)	Cement (c)	RCA	NCA	Fine aggregates	
Lab concrete	100	0.45	419	188	1125	0	659	130
	50	0.45	426	191	572	572	670	150
	0	0.45	433	194	0	1163	681	180
Demolition project	100	0.45	420	189	0	1128	661	120

aggregates. Similar test results were obtained by Manzi et al. [6]. Compared to the ideal slump values of 150–160 mm for concrete fill in CFST real projects [41], 130 mm slump of concrete with 100% RCA is relatively lower in this study. During the process of concrete filling, the RACFSTs and CFSTs were cast and vibrated in the same way to achieve uniform vibration. When the RAC is applied in real structural projects, its workability can be improved by adding a small content of superplasticizer or cement paste in RAC mixture [36,42–44]. For example, the research by Matias et al. showed that the use of only 0.5% of cement weight of high-performance superplasticizer is time-effective in achieving a desired workability for recycled aggregate concrete (RAC) [42]. This will not have great effect on the carbon footprint or cost of concrete.

Concrete cubes with the side length of 100 mm and prisms with the dimension of 150 mm × 150 mm × 300 mm were cast and cured in conditions similar to the composite specimens. The concrete cube strength and the elastics modulus were determined by testing at 28 days after concrete casting ($f_{cu100,28}$ and $E_{c,28}$) and at the time of ultimate tests of RACFST specimens ($f_{cu100,test}$ and $E_{c,test}$). Table 4 lists the mean values of material properties. Equivalent values of 150 mm concrete compressive cube strength ($f_{cu,28}$ and $f_{cu,test}$) and cylinder strength ($f_{cm,28}$ and $f_{cm,test}$) developed from conversion factors specified in the Chinese concrete code GB50010-2010 [45] and CEB-FIP Model Code 1990 [46] are also included in Table 4. The cube compressive strength decreases by 12.4% and 16.3% when the natural coarse aggregates were 100% replaced by RCA from laboratory waste concrete (RCA-L) and building demolition project (RCA-P), respectively. This is because the

aggregate-cement matrix interfacial zone of RAC consisted mainly of loose and porous hydrates due to the adhered mortar (Table 2) while that of conventional concrete consisted mainly of dense hydrates [47]. Additionally, it is observed that the elastic modulus is more sensitive to the inclusion of RCA than the compressive strength. Reductions of the 25.0% and 29.4% were noted in the tests for the elastic modulus of concrete with 100% RCA-L and RCA-P, respectively, due to the large amount of the adhered mortar with comparatively lower elastic modulus that is attached to original aggregates in RAC. The reductions on the compressive strength and elastic modulus are within the range reported in an overview of study on RAC by Xiao et al. [5].

Tensile coupon tests were performed to determine the material properties of the circular steel tubes in accordance with the Chinese Standard GB/T228-2010 [48]. Vertical and horizontal deformations were measured by strain gauges located at the mid-height of the samples on both sides, and the average yield strength (f_y), ultimate tensile strength (f_u), elastic modulus (E_s) and Poisson's ratio (μ_s) are presented in Table 5.

2.3. Preparation of RACFST specimens

A 160 mm × 160 mm × 10 mm plate was welded to the bottom of each empty steel tube. Concrete was then poured into the vertical tubes, and an external vibrator was used for compaction. The concrete was cast slightly higher than the steel tube to avoid gaps between the concrete core and the top steel tube. Once the casting was completed, the top surfaces of the concrete core were tightly wrapped and sealed with an aluminum sheet and a plastic film

Table 4
Basic properties of natural and recycled aggregate concrete.

RCA resource	r (%)	$f_{cu100,28}$ (MPa)	$f_{cu,28}$ (MPa)	$f_{cm,28}$ (MPa)	$E_{c,28}$ (×10^4 MPa)	$f_{cu100,test}$ (MPa)	$f_{cu,test}$ (MPa)	$f_{cm,test}$ (MPa)	$E_{c,test}$ (×10^4 MPa)
Lab concrete	100	42.5	40.4	33.2	2.40	54.4	51.7	41.5	2.60
	50	45.5	43.2	35.4	2.77	60.3	57.3	45.1	3.17
	0	49.2	46.7	38.1	3.13	62.1	59.0	46.4	3.47
Demolition project	100	44.7	42.5	34.8	2.23	52.0	49.4	40.0	2.45

Table 5
Basic properties of steel tubes.

Dimension of section $D \times t$ (mm^2)	Yield strength f_y (MPa)	Tensile strength f_u (MPa)	Elastic modulus E_s (×10^5 MPa)	Poisson's ratio μ_s
140 × 2.75 (α = 0.08)	299.4	337.8	1.83	0.282
140 × 3.75 (α = 0.11)	355.6	426.9	1.84	0.286
140 × 4.50 (α = 0.14)	323.8	416.7	1.78	0.268

① Specimen; ② Strain gauges; ③ Rigid sub-plate; ④ LVDT; ⑤ Load cell

— Locations for horizontal strain gauges
▌ Locations for vertical strain gauges
▸ Locations for strain gauges
⊕ Locations for LVDTs

Steel tube
RAC core

(a)

① Specimen; ② Strain gauges; ③ Sharp knife hinge; ④ LVDT

— Locations for horizontal strain gauges
▌ Locations for vertical strain gauges
▸ Locations for strain gauges
⊕ Locations for LVDTs

Steel tube
RAC core

(b)

① Specimen; ② Strain gauges; ③ Rigid beam; ④ LVDT; ⑤ Pin-end support

— Locations for horizontal strain gauges
▌ Locations for vertical strain gauges
▸ Locations for strain gauges

Steel tube
RAC core

(c)

Fig. 2. Layout of the tests for RACFST specimens.

to simulate the sealing achieved by CFST during construction and service. Prior to testing, the aluminum sheet and the plastic film were removed, the composite specimens were ground plane and smooth, and a second steel plate was welded to the top of each column.

2.4. Test setup and procedure

A load cell was used for short columns of test groups 1 and 2 with slenderness ratio λ = 12 as shown in Fig. 2(a). Slender columns under axial loading and the specimens under combined loading were tested in a special assembly with the pinned ends as shown in Fig. 2(b). The desired eccentricity was achieved by accurately machining 10 mm deep grooves into the stiff steel plates (30 mm thick), which were connected with the end steel plates of the specimens. For the pure axial compression column, the groove was in the middle of the plate. Two sharp knife edges were designed and attached to the top and the bottom plates, respectively to allow specimen rotation, to simulate pin-ended supports, and to accurately control eccentricity. The eccentricity of the applied load was equal at both ends, and the columns were subjected to single curvature bending. A three-point bending system was used to apply the moment on the RACFST beams under bending with pin-ended supports as shown in Fig. 2(c).

Longitudinal and circumferential strains were measured at four positions around the perimeter of the centre of the steel tubes by eight electrical resistance strain gauges as illustrated in Fig. 2.

Another four longitudinal strain gauges were employed to monitor the vertical deformations of the tubes at the locations 45°, 135°, 225° and 315° degrees for specimens under combined loading and the beams under flexure loading to investigate the plane-sections hypothesis.

Axial shortening of the specimens was measured by four LVDTs. Two were used to monitor the movement of the top plate, and the other two monitored the movement of the bottom plate. For the columns under combined loading, six LVDTs were used to symmetrically measure the lateral deflection of the column at the mid length (two LVDTs at 0.5L) and also one LVDT at four additional levels (0L, 0.25L, 0.75L, and 1L). For the beams under flexural loading, the in-plane vertical displacements at two trisection points, mid-span and two supports were measured by five LVDTs.

The loading rate was 2 kN/s up to approximately 85% of the expected load carrying capacity, after which the tests were loaded under displacement control in order to measure post-peak behavior of the specimens.

3. Analysis of test results

3.1. Failure modes

Fig. 3 depicts typical failure modes of the tested RACFST specimens. The stub columns under axial loading exhibited shear failures (see Fig. 3(a) and (b)) while the other columns experienced
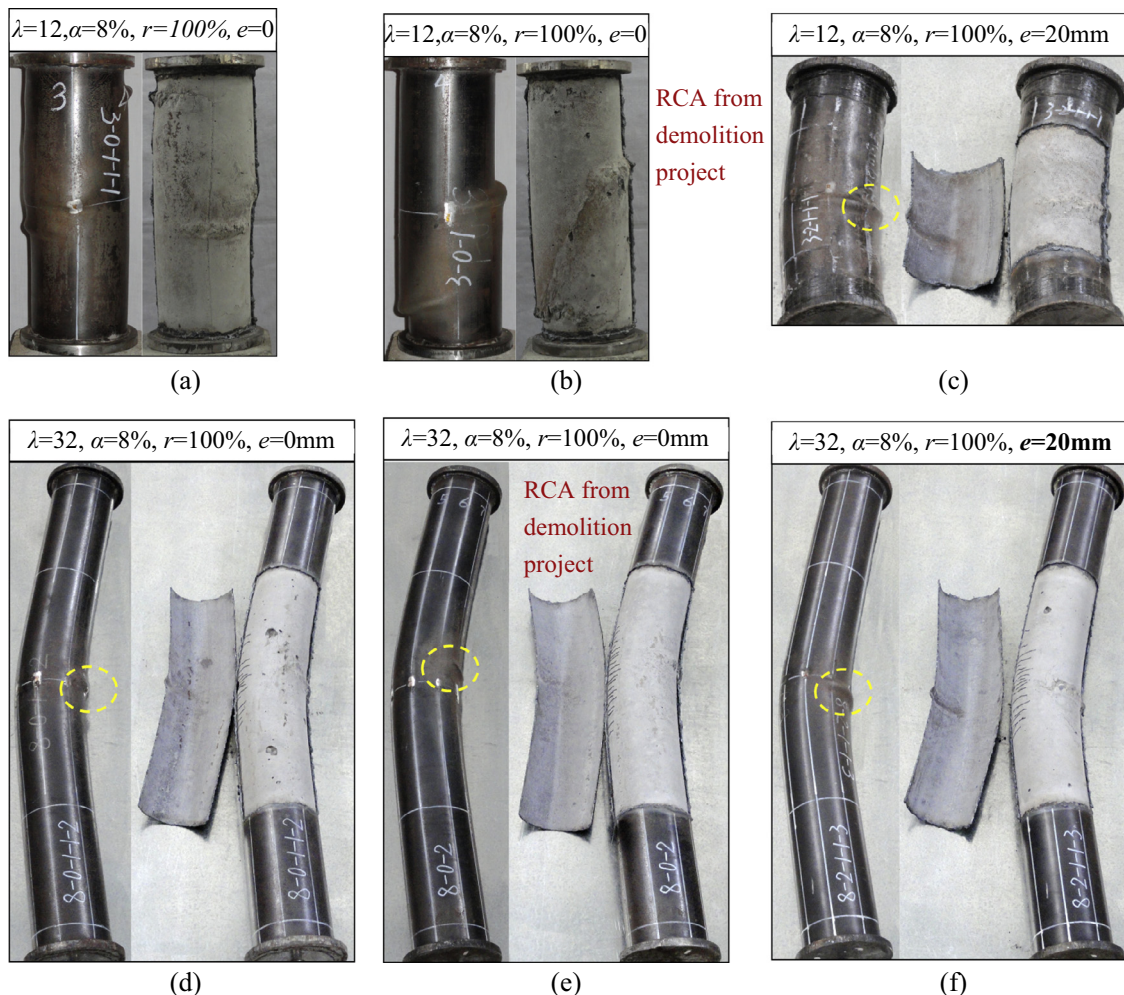

Fig. 3. Failure modes of representative specimens: (a) CL12-8-100-0-a; (b) CP12-8-100-0-c; (c) CL12-8-100-20-a; (d) CL32-8-100-0-b; (e) CP32-8-100-0-b; (f) CL32-8-100-20-c; (g) CL32-8-50-20-a; (h) CL32-8-0-20-a; (i) CL32-14-100-20-c; (j) CL32-8-100-40-c; (k) CL48-8-100-20-a and (l) CL36-8-100-∞-a, b, c.
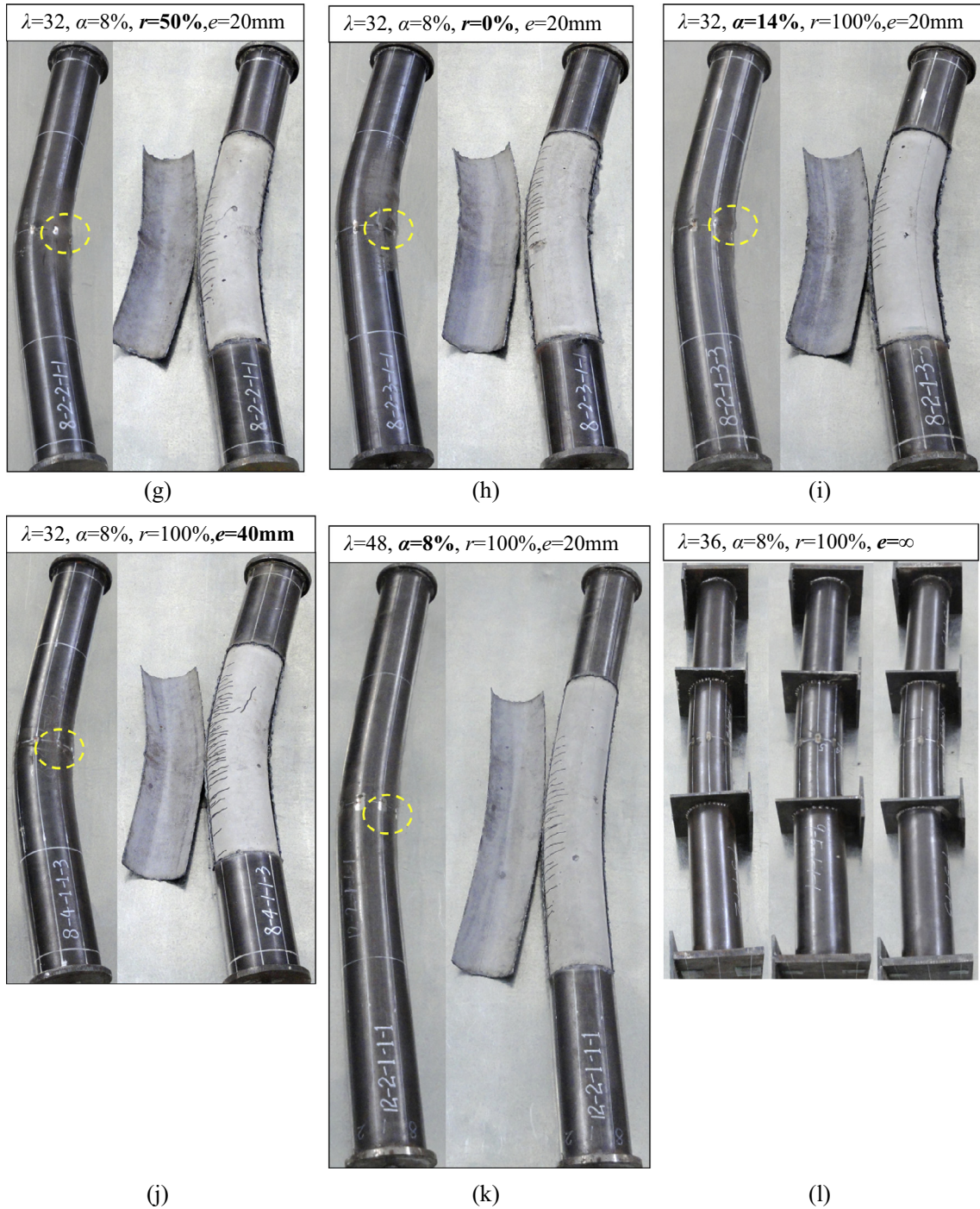
$\lambda=32$, $\alpha=8\%$, **$r=50\%$**, $e=20$mm (g)

$\lambda=32$, $\alpha=8\%$, **$r=0\%$**, $e=20$mm (h)

$\lambda=32$, **$\alpha=14\%$**, $r=100\%$, $e=20$mm (i)

$\lambda=32$, $\alpha=8\%$, $r=100\%$, **$e=40$mm** (j)

$\lambda=48$, **$\alpha=8\%$**, $r=100\%$, $e=20$mm (k)

$\lambda=36$, $\alpha=8\%$, $r=100\%$, **$e=\infty$** (l)

Fig. 3 (*continued*)

global flexural buckling failure modes (see Fig. 3(c) through (k)). The steel tubes of some typical specimens were cut and removed to investigate the influence of study parameters on the damage of the concrete cores after tests. These specimens included 9 slender columns and 3 stub columns. All the columns under combined loading failed with large lateral deflections, and buckling generally occurred near the mid-height of the specimens. This suggests that the RCA replacement percentage and source of RCA do not influence the failure mode for RACFST stub and slender columns under combined loading. The beam specimens failed in a ductile manner and no tensile fracture was observed (see Fig. 3(l)).

Fig. 3 also shows tensile flexural cracks in the concrete core of the longer columns. Table 6 summarizes the range of the cracks from the mid-height of the specimens, the maximum length and the number of cracking for the representative slender specimens with the same lateral deformation. Specimens with substantially higher RCA replacement percentage have more and bigger perpendicular cracks over a longer range from the mid-height. For example, specimens CL32-8-100-20-c and CL32-8-50-20-a have 44% and 11% more cracks, and have 20 mm and 15 mm longer cracking lengths than specimen CL32-8-0-20-a does, respectively (see Fig. 3(f)–(h) and Table 6). The RACFST specimen with aggregate

Table 6
Perpendicular cracks in the concrete core of the representative specimens.

Specimen labels	Range from the mid-height (mm)	Maximum length (mm)	Number
CL32-8-100-0-b	±110	45	16
CP32-8-100-0-b	±130	45	21
CL32-8-100-20-c	±195	80	26
CL32-8-50-20-a	±180	75	20
CL32-8-0-20-a	±173	60	18
CL32-11-100-20-b	±185	60	20
CL32-14-100-20-c	±200	55	15
CL32-8-100-40-c	±245	90	28
CL48-8-100-20-a	±260	75	22

produced from lab concrete has fewer perpendicular cracks compared to the specimen filled with concrete with aggregate produced from a real building demolition project. However, the source of RAC does not affect the maximum length of the cracks (see Fig. 3(d), (e) and Table 6). As expected, RACFST specimens with higher α ratio also have better ductility. For example, compared to specimen CL32-8-100-20-c, specimen CL32-14-100-20-c has fewer perpendicular cracks over a shorter range from the mid-height (see Fig. 3(f), (i) and Table 6). This may be due to the larger portions of resistance provided by the thicker steel tube and better confinement of the concrete provided by the steel tube. It also can be observed that the concrete suffers more serious damage with increased eccentricity (see Fig. 3(i), (j) and Table 6).

3.2. Performance indices

Figs. 4 and 5 depict the compressive load versus axial deflection and mid-span deflection, respectively, for the test specimens. In all cases, the 3 identical specimens in each group have consistent experimental results. Thus, the average value of each group is adopted in the following analysis. Table 7 shows the initial stiffness (EA), the compressive load capacity (P_u) and the corresponding scatter in each group of the column tests, the vertical displacement at maximum compressive load ($\triangle_u$), the mid-span deflection at maximum compressive load (u_m), the vertical dis-

placement at $0.85P_u$ after maximum compressive load ($\triangle_{0.85}$), and the ductility index (DI), which is a measure of deformation capacity defined in Eq. (1). The initial stiffness (EA) was determined from the test results of compressive load versus axial deflection curve.

$$DI = \frac{\Delta_{0.85}}{\Delta_u} \tag{1}$$

Consistent experimental results are also obtained for the RACFST beam tests as shown in Fig. 6. Fig. 6(a) and (b) depict the moment versus curvature and moment versus extreme fiber strain for the test specimens, respectively, where the tensile strain is positive when the compressive stain is negative in the figure. Han [49] suggests that the ultimate moment in the CFSTs under bending can be defined as the moment corresponding to an extreme tensile fiber strain of the steel tube of 0.01. According to this definition, the ultimate moment capacity of the RACFST beams measured from Fig. 6(b) is 18.55 kN m in average with the corresponding scatter of 2.1%. However, the actual average maximum moment capacity is 20.39 kN m, which is 9.9% larger than the moment at 1% strain.

Figs. 7 and 8 illustrate the compressive strain, tensile strain, centroid axis strain and the lateral deflection of the representative specimens measured at different axial load levels. These two figures suggest that the cross-section remained plane after deformation for the RACFST column and beam specimens. It also shows that the deflection curve was approximately in the shape of a half sine wave.

3.2.1. Compressive load capacity

Fig. 9 shows the influence of the replacement percentage of recycled aggregate (r), source of RCA, slenderness ratio (λ) and the α ratio on the compressive load capacity of the specimens.

The compressive load capacity of the columns has a modest decrease with increasing substitution level of RCA. For example, the maximum compressive load decreases by 11.2% and 4.5% when the natural coarse aggregates were replaced 100% RCA for the specimens with eccentricity of 20 mm and ***40 mm, respectively
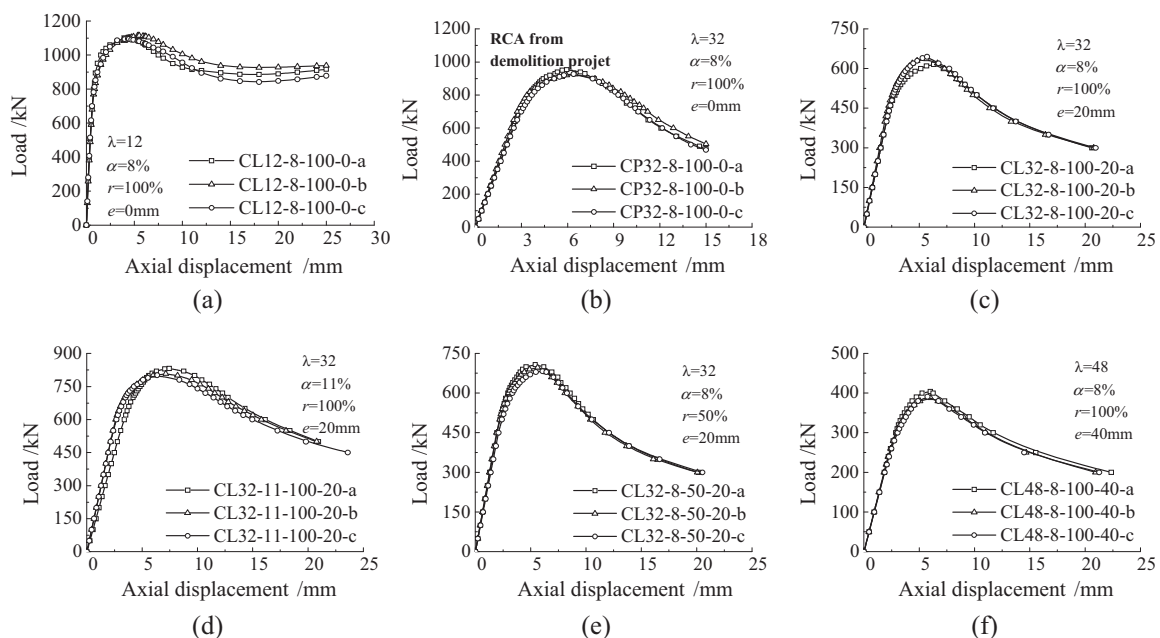

Fig. 4. Axial load versus vertical displacement curves for representative test specimens: (a) CL12-8-100-0; (b) CP32-8-100-0; (c) CL32-8-100-20; (d) CL32-11-100-20; (e) CL32-8-50-20; and (f) CL48-8-100-40.
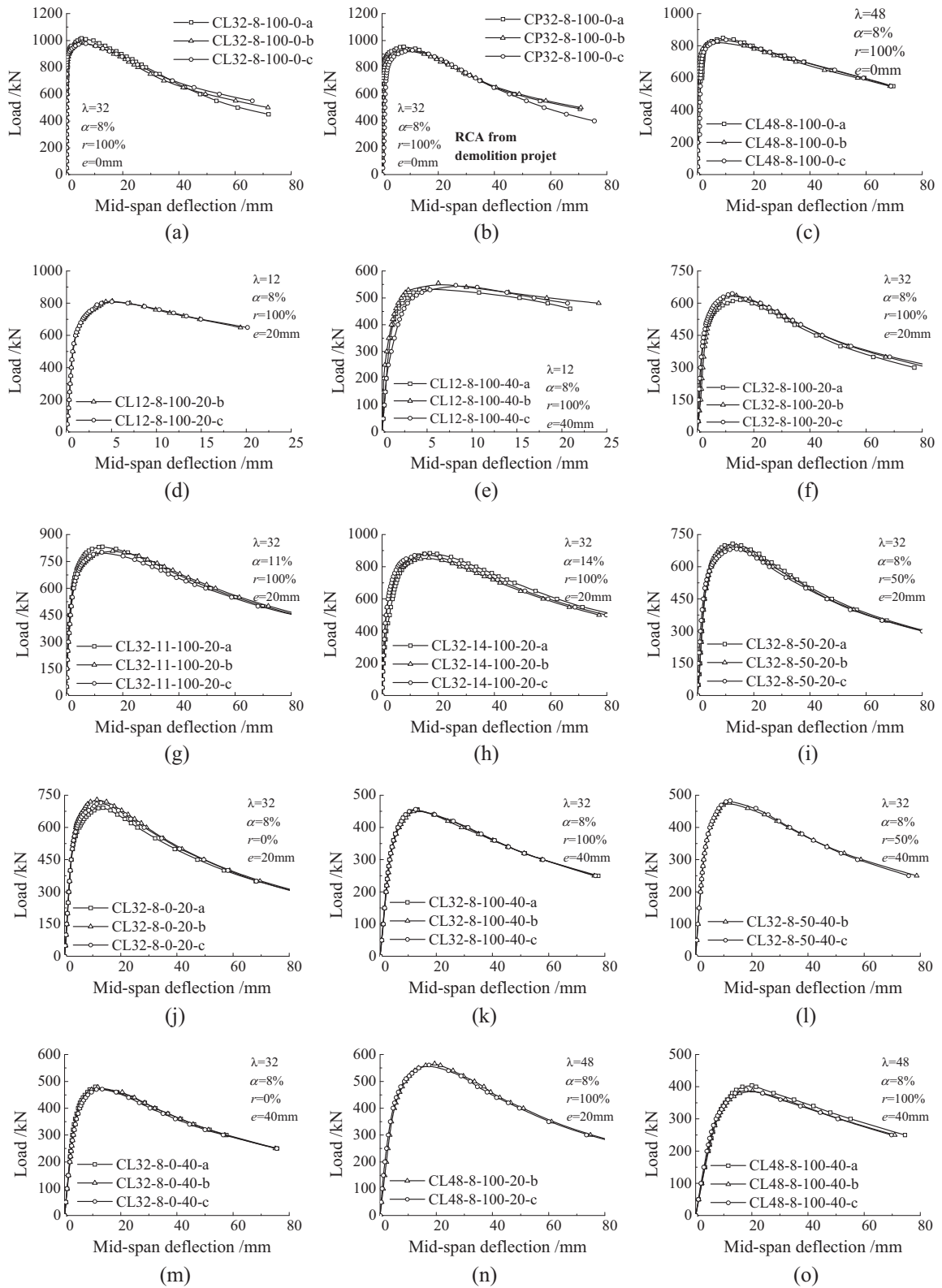
Fig. 5. Axial load versus mid-span deflection curves for all the test column specimens: (a) CL32-8-100-0; (b) CP32-8-100-0; (c) CL48-8-100-0; (d) CL12-8-100-20; (e) CL12-8-100-40; (f) CL32-8-100-20; (g) CL32-11-100-20; (h) CL32-14-100-20; (i) CL32-8-50-20; (j) CL32-8-0-20; (k) CL32-8-100-40; (l) CL32-8-50-40; (m) CL32-8-0-40; (n) CL48-8-100-20 and (o) CL48-8-100-40.

(Fig. 9(a)). The structural effects of using 100% RCA in place of natural aggregate is somewhat smaller than the corresponding material effects, since a reduction of 12.4% is noted for the cube compressive strength for 100% replacement in the tests (Table 4)

as compared to 11.2% and 4.5% for the column specimens. The scatters were less than 3% over all the test specimens (Table 7), which indicate that the contribution of the steel tube and the confinement effects may be the main reasons for reducing the scatter of

Table 7
Experimental results of RACFST columns.

Group	Specimen labels	EA (10^5 kN)		P_u (kN)		$\triangle_u$ (mm)		u_m (mm)		$\triangle_{0.85}$ (mm)	DI		P_{ce}/P_u	
1	CL12-8-100-0-a	5.29	5.28	1104	1105	4.448	(0.9%)			9.516	8.59	9.88	0.68	0.71
	CL12-8-100-0-b	5.12		1115		5.430				12.940	11.08		0.67	
	CL12-8-100-0-c	5.42		1095		4.328				10.679	9.96		0.78	
2	CP12-8-100-0-a[23]	5.74	5.34	1100	1096	3.897	(0.4%)			10.032	9.57	10.19	0.76	0.71
	CP12-8-100-0-b[23]	5.88		1092		4.700				13.540	13.37		0.73	
	CP12-8-100-0-c[23]	4.39		1095		4.817				10.070	7.63		0.64	
3	CL32-8-100-0-a	6.32	6.00	1017	992	6.500	(2.2%)	5.325	6.101	9.780	2.08	2.09	0.77	0.76
	CL32-8-100-0-b	5.96		983		5.930		6.126		8.940	1.99		0.77	
	CL32-8-100-0-c	5.72		977		6.930		6.851		10.250	2.20		0.74	
4	CP32-8-100-0-a	5.85	5.88	954	936	5.950	(1.7%)	7.686	9.301	9.110	2.09	2.25	0.82	0.76
	CP32-8-100-0-b	5.75		926		6.500		9.422		9.940	2.48		0.70	
	CP32-8-100-0-c	6.04		928		6.390		10.796		9.480	2.18		N/A	
5	CL48-8-100-0-a	5.82	5.91	850	837	5.751	(1.6%)	9.021	8.720	7.980	1.67	1.75	0.93	0.91
	CL48-8-100-0-b	5.65		824		5.288		7.042		8.210	1.84		0.96	
	CL48-8-100-0-c	6.26		837		5.564		10.098		7.850	1.73		0.84	
6	CL12-8-100-20-a	6.64	6.12	N/A	812	N/A	(0.3%)	N/A	5.064	N/A	N/A	3.41	0.68	0.66
	CL12-8-100-20-b	5.55		813		4.432		5.084		9.390	3.38		0.55	
	CL12-8-100-20-c	6.18		810		4.335		5.044		9.350	3.44		0.74	
7	CL12-8-100-40-a	6.02	6.49	535	546	4.174	(1.8%)	5.035	6.499	14.980	5.97	4.64	0.67	0.61
	CL12-8-100-40-b	6.77		555		5.964		6.264		15.940	4.17		N/A	
	CL12-8-100-40-c	6.69		547		7.104		8.199		15.340	3.77		0.55	
8	CL32-8-100-20-a	5.80	5.82	616	632	6.305	(2.4%)	15.188	13.794	9.540	2.62	2.50	0.68	0.65
	CL32-8-100-20-b	5.98		636		5.661		13.829		8.830	2.52		0.63	
	CL32-8-100-20-c	5.68		645		5.706		12.366		8.960	2.36		0.65	
9	CL32-11-100-20-a	7.25	7.10	832	814	7.437	(2.7%)	12.769	13.914	12.590	2.43	2.73	0.72	0.73
	CL32-11-100-20-b	7.21		808		7.141		16.417		12.600	3.16		0.75	
	CL32-11-100-20-c	6.85		801		6.372		12.558		12.050	3.04		0.73	
10	CL32-14-100-20-a	8.35	8.01	884	873	8.859	(1.8%)	16.984	16.277	14.490	2.63	2.88	0.83	0.82
	CL32-14-100-20-b	7.57		855		7.429		16.660		12.570	3.08		0.78	
	CL32-14-100-20-c	8.13		880		7.289		15.187		12.430	2.93		0.84	
11	CL32-8-50-20-a	6.59	6.79	708	696	5.404	(1.8%)	12.442	13.345	8.530	2.40	2.38	0.56	0.68
	CL32-8-50-20-b	7.05		697		5.628		13.757		8.270	2.39		0.69	
	CL32-8-50-20-c	6.73		683		6.080		13.836		8.660	2.34		0.79	
12	CL32-8-0-20-a	7.85	7.52	692	712	5.395	(2.7%)	13.664	12.711	7.950	2.53	2.47	0.69	0.70
	CL32-8-0-20-b	7.49		730		5.068		11.532		8.080	2.37		0.68	
	CL32-8-0-20-c	7.22		715		5.569		12.938		8.680	2.52		0.73	
13	CL32-8-100-40-a	5.92	5.70	456	455	5.641	(0.4%)	13.293	13.154	10.640	3.01	2.97	N/A	0.63
	CL32-8-100-40-b	5.70		453		5.790		13.526		10.610	2.86		0.68	
	CL32-8-100-40-c	5.48		456		5.478		12.643		10.790	3.05		0.57	
14	CL32-8-50-40-a	6.71	6.87	N/A	480	N/A	(0.9%)	N/A	12.176	N/A	N/A	2.89	0.56	0.65
	CL32-8-50-40-b	7.09		477		5.089		12.093		9.690	2.83		0.63	
	CL32-8-50-40-c	6.82		483		5.506		12.258		10.350	2.95		0.75	
15	CL32-8-0-40-a	7.63	7.35	480	477	4.901	(1.0%)	10.913	12.034	9.770	2.99	2.87	0.79	0.65
	CL32-8-0-40-b	7.40		479		5.071		11.787		9.610	2.78		0.58	
	CL32-8-0-40-c	7.02		471		5.552		13.403		9.490	2.86		0.59	
16	CL48-8-100-20-a	5.98	6.19	566	564	5.567	(0.6%)	19.426	18.409	7.720	1.99	1.98	0.64	0.67
	CL48-8-100-20-b	6.38		N/A		N/A		N/A		N/A	N/A		0.63	
	CL48-8-100-20-c	6.20		561		5.450		17.391		7.820	1.96		0.75	
17	CL48-8-100-40-a	6.68	6.15	404	394	6.001	(2.2%)	20.051	19.412	9.330	2.19	2.21	0.69	0.61
	CL48-8-100-40-b	6.30		388		6.044		20.236		9.510	2.31		0.52	
	CL48-8-100-40-c	5.49		391		5.754		17.950		9.220	2.14		0.61	

Note: The value in the bracket is the coefficient of variation of the maximum compressive loads in each group.

the test results. This observation encourages the use of RACFSTs in structural engineering and the sustainable environmental benefits that result. Similar results were obtained for RACFST stub column tests under axial loading by the authors [23].

A challenge to using large volumes of recycled aggregates is the inherent variability of the waste materials. Significant variation in performance has been seen in previous research, and this variation is a function of the source and type of aggregate [50,51]. Fig. 9(b) shows that the RACFST specimens with the two different RCAs produced from the lab and the demolition project have basically the same load capacities, with only 0.8% and 5.6% differences for the specimens with slenderness ratio of 12 and 32, respectively. It is anticipated that the similar size grading and index of crushing obtained in the aggregates and the same mix proportioning method adopted in the experiments may have contributed to this benefit. Thus, the tests on the size grading and physical properties for RCAs are recommended for the application of RACFST. Further work may be required to study the effects of the source of RCA on the performance of RACFST composite columns, since this finding is in some conflict with other observations. In addition, RCA obtained from commercial sources may be contaminated with organic materials during the crushing process. These impurities
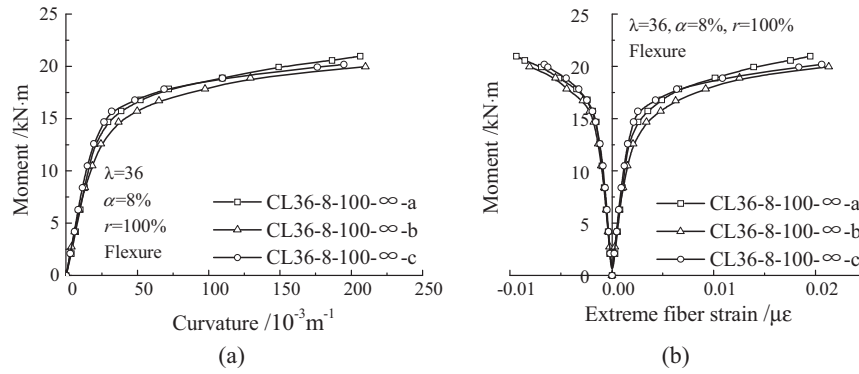
Fig. 6. Test results of the beam tests: (a) moment versus curvature; and (b) moment versus extreme fiber strain.
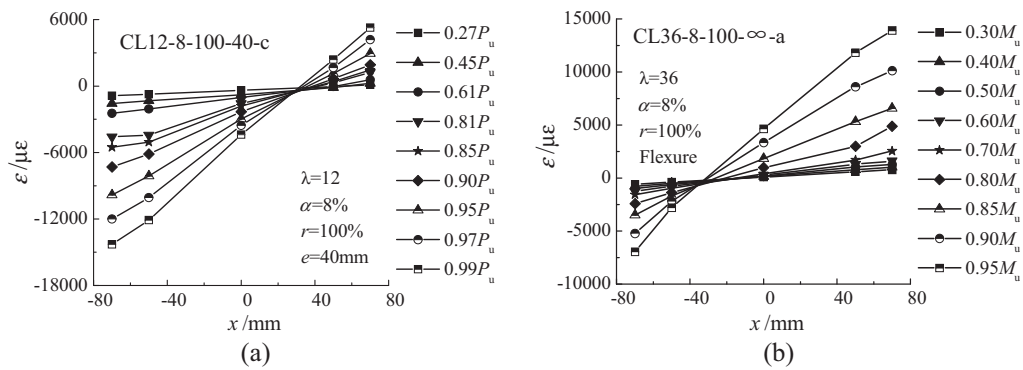

Fig. 7. Distribution of the strain across the section of the mid-height of representative specimens: (a) CL12-8-100-40-c; and (b) CL36-8-100-∞-a.
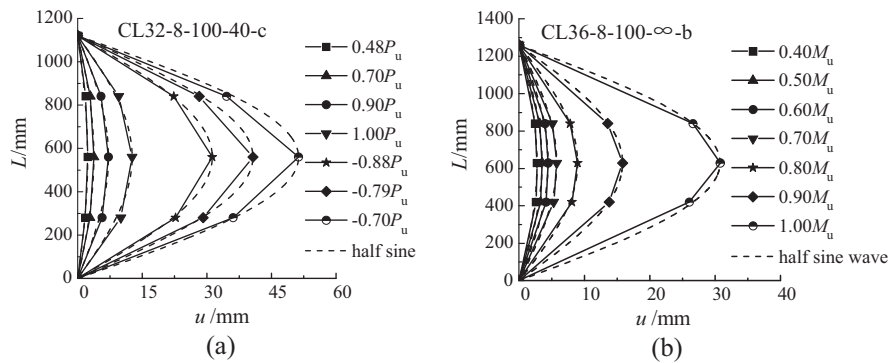

Fig. 8. Lateral deflection curves of representative specimens: (a) CL32-8-100-40-c; and (b) CL36-8-100-∞-b.

may reduce the strength, elastic modulus and deteriorate the durability performance for RAC. Therefore, further study may also be suggested to investigate the effects of the content of organic materials in RCA on the long-term behavior of RACFST composite columns.

Fig. 9(c) shows the influence of the slenderness ratio (λ) and eccentricity (e) on the static compressive resistance of RACFST columns. As expected, RACFST specimens with higher ratio λ and eccentricity have lower maximum compressive loads, because of secondary moments and stability effects. The stub columns with slenderness ratio of 12 attained their ultimate yield and concrete crushing capacity, while those slender columns with slenderness ratios of 32 and 48 only attained 77.9%–89.8% and 69.4–75.7% of this ultimate capacity, respectively. Reductions of 50.6–54.1% are observed for the RACFST columns with eccentricity of 40 mm com-

pared to those under concentric loading. The calculation of critical buckling load (P_{cr}) was based on the nominal sectional strength (P_o) and the relative slenderness ratio ($\bar{\lambda}$) which is considered the length slenderness effects in AISC [28]. Based on the AISC provisions, P_{cr} can be determined by Eqs. (2)–(5). The relationship of P_u/P_0 with $\bar{\lambda}$ compared to the corresponding curves in AISC [28] are plotted in Fig. 10. The figure shows that the experimental trends with higher relative slenderness ratio are similar to the theoretical line in AISC. This may be attributed to the more considerable confinement effects acting for the short columns and the different loading conditions for the short and slender columns as shown in Fig. 2.

$$P_{cr}/P_0 = 0.658^{\bar{\lambda}^2} \quad \text{when} \quad \bar{\lambda} \leqslant 1.5 \qquad (2)$$
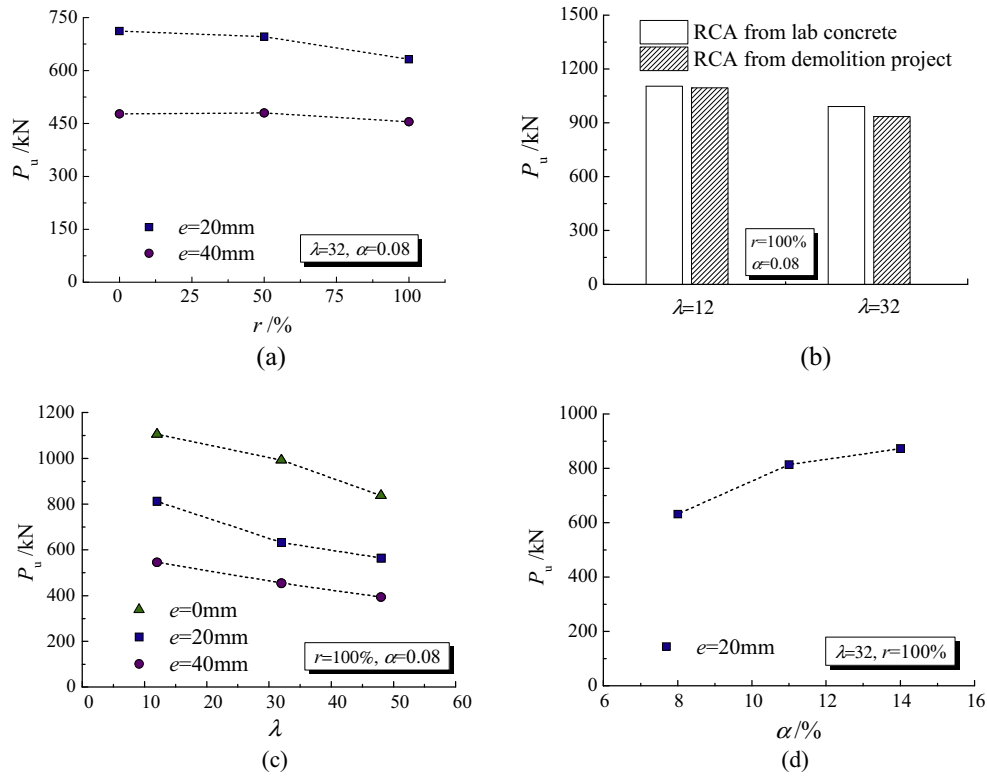
Fig. 9. Compressive load capacity of test specimens with different (a) RCA replacement ratios; (b) RCA sources; (c) slenderness ratios and (d) steel to concrete area ratios.
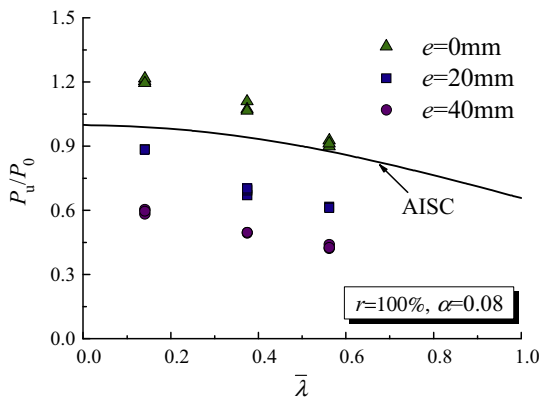

Fig. 10. Relationship of P_u/P_0 with relative slenderness ratio compared to the corresponding curve in AISC.

$$P_{cr}/P_0 = 0.877/\overline{\lambda}^2 \quad \text{when} \quad \overline{\lambda} > 1.5 \tag{3}$$

$$P_0 = 0.95 f_{cm} A_c + f_y A_s \tag{4}$$

$$\overline{\lambda} = \sqrt{\frac{P_0}{\pi^2 EI_{eff}/(kL)^2}} \tag{5}$$

The influence of the α ratio on the maximum compressive load of slender RACFST columns under eccentric loading is plotted in Fig. 9(d). As expected, significant increases in the maximum compressive load for the specimen occurred with higher α ratio. Confinement effects acting on the specimens with different α ratios can be evaluated and compared in terms of the strength index

P_u/P_0. This index for the group CL32-14-100-20 and CL32-11-100-20 is 10.4% and 6.3% higher than that for the group CL32-8-100-20 (see Fig. 11).

3.2.2. Initial stiffness

The initial stiffness of the specimens as a function of the replacement percentage of RCA (r), source of RCA and the α ratio are illustrated in Fig. 12. Compared to the test results in Fig. 9(a), it is observed that the initial stiffness is more sensitive to the inclusion of RCA than the compressive load capacity, since decreases in the value of the initial stiffness of columns are 22.6% and 22.5% in maximum for the specimens with eccentricity of 20 mm and 40 mm, respectively (see Fig. 12(a)) as compared to 11.2% and 4.5% for the compressive load capacity of the columns (see Fig. 9 (a)). Fig. 12(a) also suggests a smaller reduction in stiffness as compared to 25.6% decrease that measured in elastic modulus for the RAC samples. The lower stiffness of the RACFST columns results

Fig. 11. Relationship of P_u/P_0 with α ratio for the test specimens.
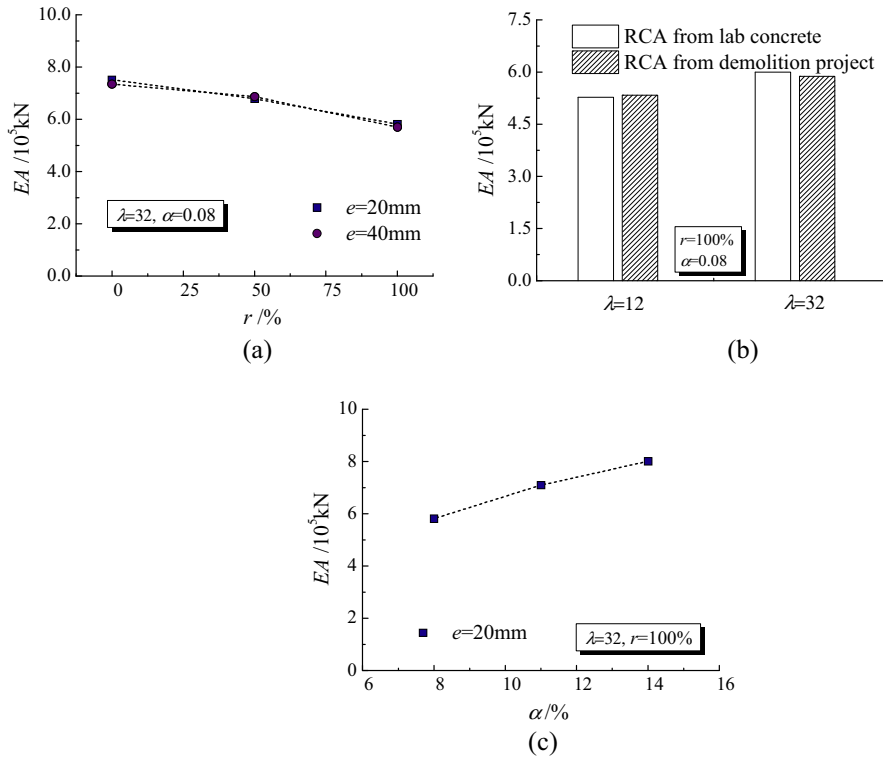
Fig. 12. Initial stiffness of test specimens with different (a) RCA replacement ratios; (b) slenderness ratios and (c) steel to concrete area ratios.
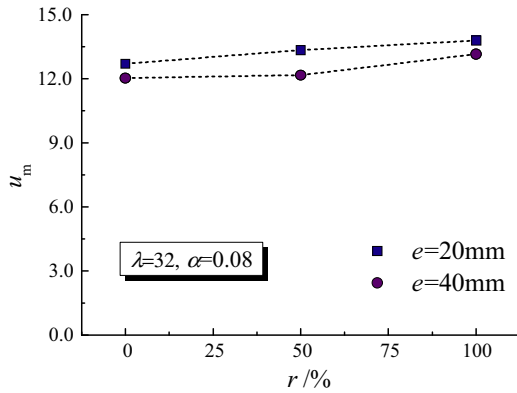

Fig. 13. Influences of RCA replacement ratio and eccentricity on mid-span deflection at maximum compressive load.

in a higher value in the mid-span deflection at compressive load capacity (u_m) with increases of 8.5% and 9.3% for 100% replacement RACFST specimens with 20 mm and 40 mm eccentricity, respectively compared to CFST columns as shown in Fig. 13.

The source of RCA had little effect on the initial stiffness as only 1.2% and 2.0% differences are observed for the specimens with slenderness ratio of 12 and 32 in Fig. 12(b), respectively. As expected, the initial stiffness increases by 22.0% and 37.6% respectively when increasing the α ratio from 8% to 11% and 14% due to the increased contribution of steel tube (see Fig. 12(c)).

3.2.3. Ductility index

Fig. 14 shows the influence of several parameters on the ductility index of the specimens. The RCA replacement ratio and its source had no significant influence on the ductility index of speci-

mens as shown in Fig. 14(a) and (b). The ductility is reduced with the increasing the slenderness ratio due to stability effects rather than material failure as shown in Fig. 14(c). This is consistent with prior observations of Yu et al. [52] and Portolés et al. [53] who examined the influence of slenderness ratio and eccentricity on the static response of CFST columns under combined loading. Fig. 14(d) shows that the specimens with higher α ratio have increased ductility because of the increased effect of the steel.

3.2.4. Confinement effects

The vertical and circumferential strains ($\varepsilon_{s,v}$ and $\varepsilon_{s,c}$) in the steel tube are used to evaluate the confinement of the concrete core produced by the steel tube. Fig. 15 depicts the ratio $\varepsilon_{s,c}/\varepsilon_{s,v}$ in the steel tubes during tests of representative specimens and the steel coupons (μ_{steel}). The load resisted by composite columns corresponding to the onset of confinement effects (P_{ce}) can be determined when the coefficient $\varepsilon_{s,c}/\varepsilon_{s,v}$ of the specimens begin to exceed the value of μ_{steel} at the same vertical deformation. The range of this interface is provided in the figure and the P_{ce}/P_u ratios for all test specimens are listed in Table 7.

The onset of confinement (P_{ce}/P_u) generally decreases with the increasing RCA content for RACFST slender columns (see Fig. 16 (a)) as observed for RACFST stub column tests by the authors [23], because of the faster rates in the progressive development of micro-cracks and the increases of strain for RAC with residual old mortar in aggregates than those for conventional concrete. The increased strains result in an earlier restraint on the transverse expansion of the concrete core by the outer tube for RACFST columns. Fig. 16(b) indicates that the specimens produced from different sources of RCA have the same load ratio P_{ce}/P_u.

Significant increase for the load ratio P_{ce}/P_u can be seen in Fig. 16(c) with the increasing slenderness ratio for the specimens under axial loading ($e = 0$ mm). Nevertheless, the load ratio P_{ce}/P_u does not seem to be greatly affected by the slenderness ratio for the specimens under eccentric loading due to the dominant sec-
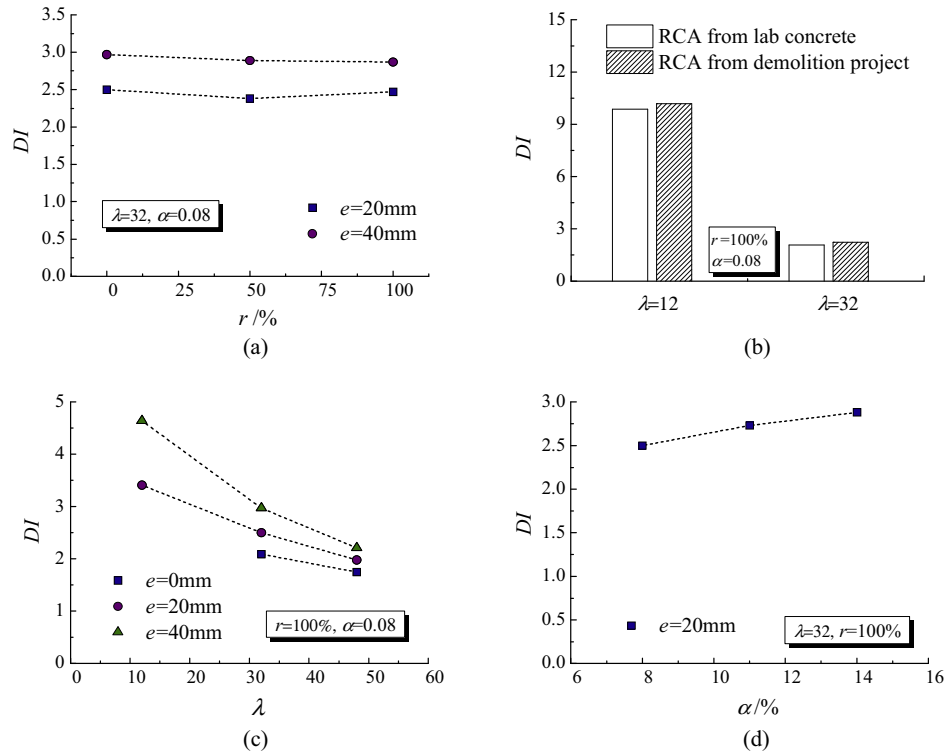
Fig. 14. Ductility index of test specimens with different (a) RCA replacement ratios; (b) RCA sources; (c) slenderness ratios and (d) steel to concrete area ratios.
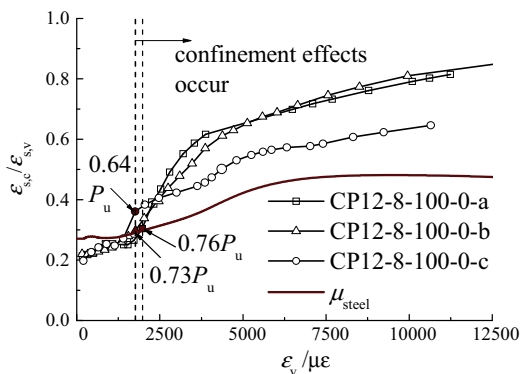

Fig. 15. Development of ratio of measured circumferential deformation ($\varepsilon_{s,c}$) over the vertical one ($\varepsilon_{s,v}$) during the tests for the typical specimens CP12-8-100-0.

ondary moments and stability effects (e = 20 mm and 40 mm). Fig. 16(c) also reveals that the load ratio P_{ce}/P_u decreases with the increasing eccentricity. It can be observed in Fig. 16(d) that the onset of confinement effects occurs later for the specimen with higher α ratio, as a result of the larger percentage of the load sustained by the steel tube.

Fig. 17(a) and (b) shows the influence of RCA replacement ratio (r) on the development of circumferential strain with the load ratio (P/P_u) for the specimens with eccentricity of 20 mm and 40 mm, respectively. The development of circumferential strain in the figure is the average value of the three specimens in each group. The figures show that larger circumferential strains were measured for the specimens with higher RCA replacement ratio during the loading process before reaching the compressive load capacity. This indicates that the larger confining pressure developed and this increased the strength enhancement in RACFST specimens more

than that in CFST specimens. This can be one of the reasons that contribute to the small difference in the compressive load capacity between the RACFST and CFST specimens as noted in Fig. 9(a).

The test results in this study initiate that the use of concrete filled steel tubes is an ideal application for RAC because the composite behavior of the member and the high strength and stiffness of the steel tube can limit the detrimental effects caused by RAC.

4. Comparison with design methods and design recommendations

The experimental research shows that the incorporation of recycled aggregate leads to a reduction of approximately 10% in compressive load capacity for RACFST columns under combined loading. As the present design codes are not yet available for RACFST columns, the different design models for predicting the performance of circular CFST members under combined loading are therefore compared to the test results to demonstrate the accuracy and the statistical variability of the various models for RACFST members. The considered design provisions include EC4 (EN 1994-1-1 [27]) in Europe, AISC (AISC 360-10 [28]) in US, and GB (GB50936-2013 [29]) in China. The database compiled consists of 45 circular RACST columns with RCA replacement ratios of 50% and 100% in this study and 12 circular RACST columns with RCA replacement ratios of 25% and 50% reported by Yang and Han [24]. The test results by Chen et al. [25,26] were excluded in the evaluation due to some failures near the end of the specimens in the tests, which suggest that there was a flaw in the eccentrically loaded boundary for some of those tests. Fig. 18 presents the comparisons of the test results with the predicted ones by various design models. Roeder et al. [12] recommended that the plastic-stress distribution method is a simple and effective method to predict the strength of circular CFST components under combined loading. Thus, only the plastic-stress distribution method was
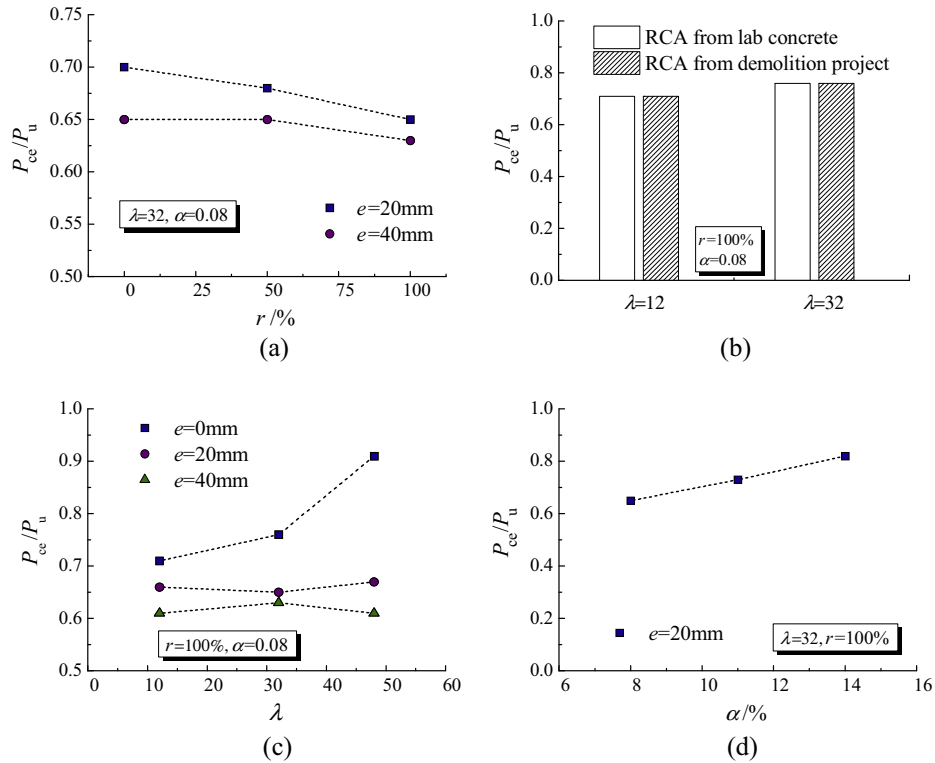
Fig. 16. Onset of confinement effects of test specimens with different (a) RCA replacement ratios; (b) RCA sources; (c) slenderness ratios and (d) steel to concrete area ratios.
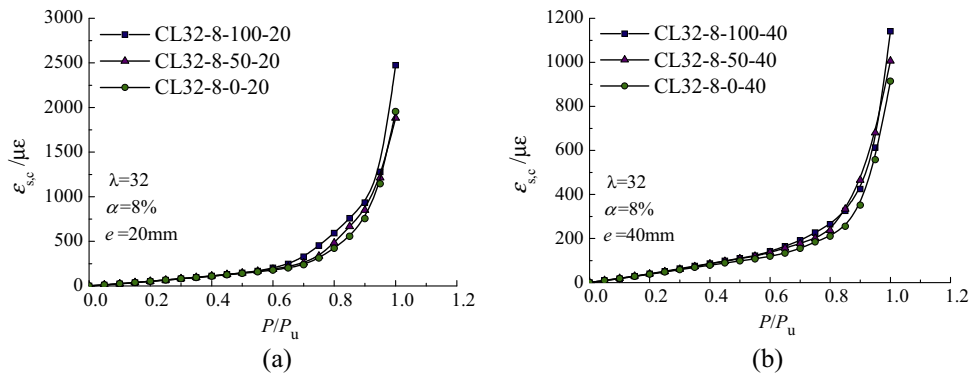

Fig. 17. Influence of RCA replacement ratio on the development of circumferential strain with load ratio for the specimens with eccentricity of (a) 20 mm and (b) 40 mm.

adopted when using the design methods of AISC and EC4 and the effect of global buckling was also considered. As the GB provides two methods, they are abbreviated as GB-1 and GB-2, respectively. The comparisons show that the available design codes are generally adequate for predicting the resistances of RACSFT columns under combined loading. In particular, EC4 and GB provide close predictions to the test results as the regression lines are close to the lines passing through the origin with a unit slope (the black solid line shown in Fig. 18) while AISC gives only 6.7% underestimation compared to the measured results.

Fig. 19 compares the calculated axial load-moment strength interaction curves (P-M) based on the various design provisions and with the test results in this paper and Refs. [18,24]. The properties of recycled aggregates in Refs. [18,24] meet the requirements for type II RCA in RILEM TC 121-DRG [30]. The average test results of the RACFST beam specimens under bending in each group of this

paper and Ref. [18] are also included in the figure (1 group of 3 specimens in this paper and 2 groups of 4 specimens in Ref. [18]). The comparisons show that EC4 and AISC provide accurate predictions of strength and GB overestimates the moment capacity for the columns under bending compared to the test results.

In the practical application of RACFSTs, the designers would pay attention to the consistency and the performance of RAC since the aggregates used may come from various sources. Thus, it suggests that the design recommendations proposed in this study can be applied for RACFSTs when the aggregates meet the requirements of Type II RCA in RILEM TC 121-DRG [30]. Additionally, the use of higher strength concrete is more practical for CFSTs to achieve better economic benefits. More experiments on RACFSTs with higher strength concrete under combined loading are therefore suggested to be performed to further validate the reliability of design recommendations proposed in this study.
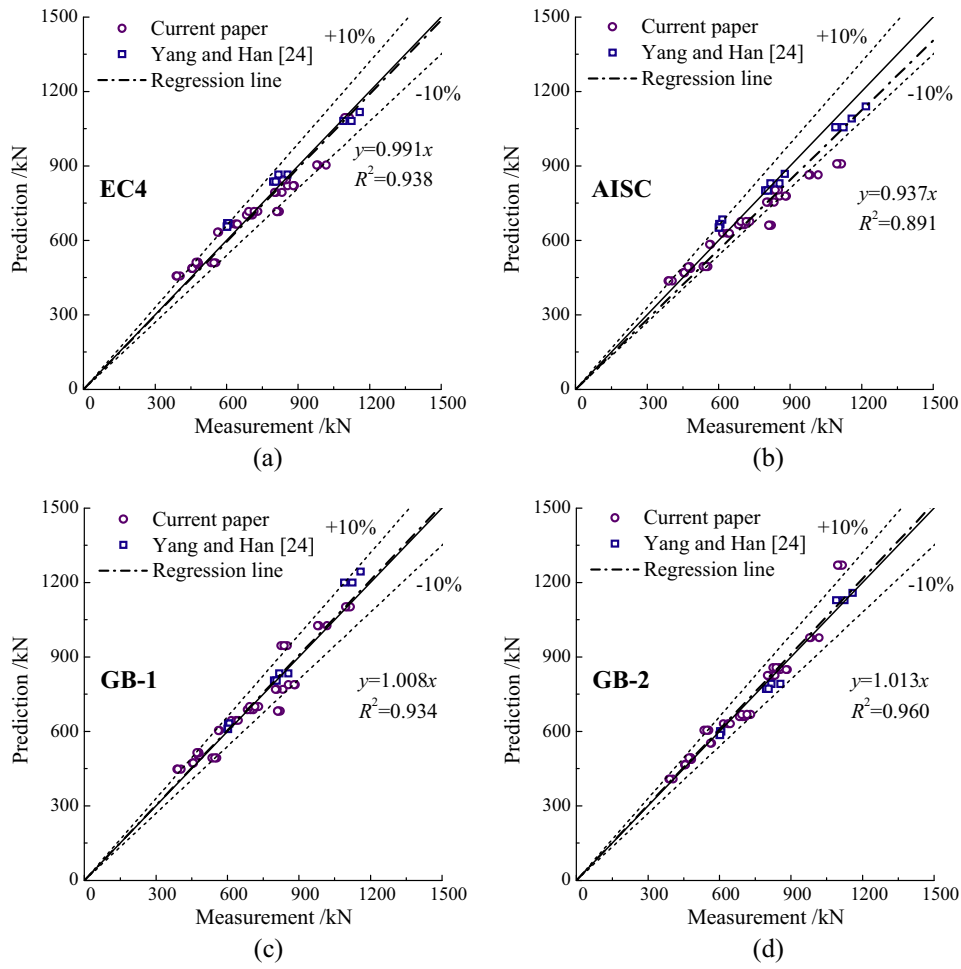
Fig. 18. Comparison of calculated and experimental compressive capacity of RACFST column tests (dot-dashed lines represent regression lines): (a) EC4; (b) AISC; (c) GB-1; and (d) GB-2.
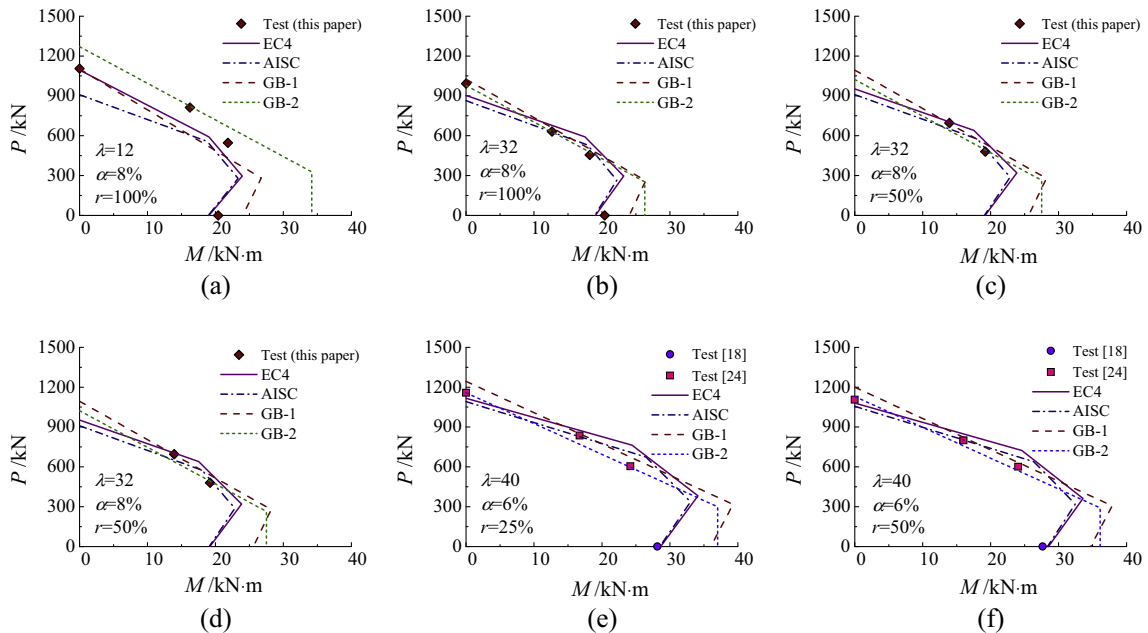

Fig. 19. Comparison of calculated and experimental axial load-moment strength interaction curves of RACFST specimen tests in this paper ((a)–(d)) and in Refs. [18,24] ((e)–(f)).

Table A1
Classification of recycled coarse aggregates for concrete (RCA).

Mandatory requirements	RCA Type I	RCA Type II	RCA Type III[e]	Test method
Min. dry particle density (kg/m^3)	1500	2000	2400	ISO 6783&7033
Max. water absorption (%)	20	10	3	ISO 6783&7033
Max. content of material with SSD < 2200 kg/m^3 (%)[a]	–	10	10	ASTM C123
Max. content of material with SSD < 1800 kg/m^3 (%)[a]	10	1	1	ASTM C123
Max. content of material with SSD < 1000 kg/m^3 (%)[a]	1	0.5	0.5	ASTM C123
Max. content of foreign materials (metals, glass, soft material, bitumen) (%)	5	1	1	Visual
Max. content of metals (%)	1	1	1	Visual
Max. content of organic material (%)	1	0.5	0.5	NEN5933
Max. content of filler (<0.063 mm) (%)	3	2	2	prEN 933-1
Max. content of sand (<4 mm) (%)[b]	5	5	5	prEN 933-1
Max. content of sulfate (%)[c]	1	1	1	BS 812, part 118
Max. allowable strength class[d]	C16/20	C50/60	No limit	–

[a] Water saturated surface dry condition (SSD).

[b] If the maximal allowable content of sand is exceeded, this part of the aggregates shall be considered together with the total sand fraction.

[c] Water soluble sulfate content calculated as SO_3.

[d] The strength class for concrete is in accordance with Eurocode 2.

[e] The composition of type III aggregates shall meet the following additional requirements: (a) the minimum content of natural aggregates is at least 80% and (b) the maximum content of type I aggregates is 10%.

5. Conclusions

In this study, the behavior of RACFST columns under combined loading and the flexure behavior of RACFST beams with normal-strength concrete under bending were studied. A total of 48 circular RACFST columns and 3 beams were tested to failure with 17 groups of 3 identical specimens. The study parameters included RCA replacement percentage, source of RCA, eccentricity ratio, slenderness ratio and the ratio of concrete area to steel area.

In all cases, the 3 identical specimens have consistent experimental results with scatter of less than 3% in each group. The contribution of the steel tube and the confinement effects may be the main reasons for the small scatter of the test results. The incorporation of the RAC has modest effect on the maximum compressive load of the RACFST columns since reductions of only 4.5–11.2% were measured in the tests for the columns with 100% RCA replacement compared to the CFST specimens. The structural effects of the replacement of recycled aggregate are somewhat smaller than the corresponding effects noted in material property tests. Similar to this, the reduction in initial stiffness in RACFST columns is smaller than that measured from material tests on the RAC samples. As part of this work, the onset of confinement are studied and it reveals that increasing RCA content for RACFST slender columns decreases the load ratio corresponding to the onset of the confinement effects.

The differences in the maximum compressive load and initial stiffness of RACFST columns with two RCA sources under combined loading are only up to 5.6% and 2.0%, respectively. These observations are different from some conclusions in the prior research for RAC. It is anticipated that the similar size grading and index of crushing obtained in the aggregates may have contributed to this benefit. Thus, the tests on the size grading and physical properties for RCAs are recommended for the application of RACFSTs. Further work may be required to study the effects of the source of RCA and its content of organic materials on the performance of RACFST composite columns.

The effects of eccentricity ratio, slenderness ratio and the steel to concrete area ratio on the behavior of RACFST columns are similar to those on the static response of CFST columns. These observations in the tests encourage the use of RACFST in structural engineering and the sustainable environmental benefits that results.

The results of 57 columns and 7 beams with normal-strength concrete in this study as well as the prior research were used to evaluate applicability of current CFST design provisions for predicting the behavior of RACFSTs. It is recommended that EC4 method provides close prediction to all the available test results for RACFST columns under combined loading and RACFST beams under bending with normal-strength concrete. This design recommendations proposed in this study can be applied for RACFSTs when the aggregates meet the requirements of Type II RCA in RILEM TC 121-DRG. This study also highlighted the need to perform further tests on RACFSTs with higher strength concrete to improve the reliability of the proposed design recommendations.

Acknowledgements

Appendix A

See Table A1.

References

[1] Breccolotti M, Materazzi AL. Structural reliability of eccentrically-loaded sections in RC columns made of recycled aggregate concrete. Eng Struct 2010;32:3704–12.

[2] Dobbelaere G, de Brito J, Evangelista L. Definition of an equivalent functional unit for structural concrete incorporating recycled aggregates. Eng Struct 2016;122:196–208.

[3] Choi WC, Yun HD. Compressive behavior of reinforced concrete columns with recycled aggregate under uniaxial loading. Eng Struct 2012;41:285–93.

[4] Eexberria M, Vázquez E, Marí A, Barra M. Influence of amount of recycled coarse aggregates and production process on properties of recycled aggregate concrete. Cem Concr Res 2007;37:735–42.

[5] Xiao JZ, Li WG, Fan YH, Huang X. An overview of study on recycled aggregate concrete in China (1996–2011). Constr Build Mater 2012;31:364–83.

[6] Manzi S, Mazzotti C, Bignozzi MC. Short and long-term behavior of structural concrete with recycled concrete aggregate. Cem Concr Comp 2013;37:312–8.

[7] Silva RV, de Brito J, Dhir RK. Comparative analysis of existing prediction models on the creep behaviour of recycled aggregate concrete. Eng Struct 2015;100:31–42.

[8] Han LH, Wang WD, Zhao XL. Behaviour of steel beam to concrete-filled SHS column frames: finite element model and verifications. Eng Struct 2008;30:1647–58.

[9] Portolés JM, Romero ML, Filippou FC, Bonet JL. Simulation and design recommendations of eccentrically loaded slender concrete-filled tubular columns. Eng Struct 2011;33:1576–93.

[10] Moon J, Roeder CW, Lehman DE, Lee HE. Analytical modeling of bending of circular concrete-filled steel tubes. Eng Struct 2012;42:349–61.

[11] Han LH, Li W, Bjorhovde R. Developments and advanced applications of concrete-filled steel tubular (CFST) structures: members. J Constr Steel Res 2014;100:211–28.

[12] Stephens MT, Lehman DE, Roeder CW. Design of CFST column-to-foundation/cap beam connections for moderate and high seismic regions. Eng Struct 2016;122:323–37.

[13] Lai MH, Ho JCM. A theoretical axial stress-strain model for circular concrete-filled-steel-tube columns. Eng Struct 2016;125:124–43.

[14] Wang YY, Geng Y, Ranzi G, Zhang SM. Time-dependent behavior of expansive concrete-filled steel tubular columns. J Constr Steel Res 2011;67:471–83.

[15] Liu H, Wang YX, He MH, Shi YJ, Waisman H. Strength and ductility performance of concrete-filled steel tubular columns after long-term service loading. Eng Struct 2015;100:308–25.

[16] Geng Y, Wang YY, Chen J. Time-dependent behavior of recycled aggregate concrete-filled steel tubular columns. J Struct Eng-ASCE 2015;141:04015011.

[17] Geng Y, Wang YY, Chen J. Time-dependent behaviour of steel tubular columns filled with recycled coarse aggregate concrete. J Constr Steel Res 2016;122:455–68.

[18] Yang YF, Han LH. Compressive and flexural behavior of recycled aggregate concrete filled steel tubes (RACFST) under short-term loadings. Steel Compos Struct 2006;6:257–84.

[19] Liu YX, Zha XX, Gong GB. Study on recycled-concrete-filled steel tube and recycled concrete based on damage mechanics. J Constr Steel Res 2012;71:143–8.

[20] Hou M, Li L, Dong JF, Wang QY. Influence of amount of recycled coarse aggregate on mechanical properties of steel tube columns. Adv Mater Res 2013;647:748–52.

[21] Chen ZP, Xu JJ, Xue JY, Su Y. Performance and calculations of recycled aggregate concrete-filled steel tubular (RACFST) short columns under axial compression. Int J Steel Struct 2014;14:31–42.

[22] Niu HC, Cao WL. Full-scale testing of high-strength RACFST columns subjected to axial compression. Mag Concrete Res 2015;67(5):257–70.

[23] Wang YY, Chen J, Geng Y. Testing and analysis of axially loaded normal-strength recycled aggregate concrete filled steel tubular stub columns. Eng Struct 2015;86:192–212.

[24] Yang YF, Han LH. Experimental behavior of recycled aggregate concrete filled steel tubular columns. J Constr Steel Res 2006;62:1310–24.

[25] Chen ZP, Li QL, Zhang XG, Xue JY, Chen BC. Mechanical behavior and bearing capacity calculation of recycled aggregate concrete-filled circular steel tube columns under eccentric loading. China Civil Eng J 2012;45:72–80 [in Chinese].

[26] Zhang XG, Chen ZP, Xue JY, Su YS, Fan J. Experimental study and mechanical behavior analysis of recycled aggregate concrete filled steel tubular long columns under axial compression. J Build Struct 2012;33:12–20 [in Chinese].

[27] European Committee for Standardization (CEN). EN 1994-1-1 Eurocode 4, Design of composite steel and concrete structures-part 1–1: general rules and rules for buildings. Brussels: CEN; 2004.

[28] American Institute of Steel Construction (AISC). AISC 360-10 Specification for structural steel buildings. Chicago (IL): AISC; 2010.

[29] Ministry of Housing and Urban-Rural Development of the People's Republic of China (MOHURD). GB50936-2013 Code for design of concrete filled steel tubular structures. Beijing: China Architecture & Building Press; 2014 [in Chinese].

[30] RILEM Technical Committee (RILEM TC). RILEM TC 121-DRG Specification for concrete with recycled aggregates. Mater Struct 1994;27:557–9.

[31] Grubl P, Ruhl M. German committee for reinforced concrete (Dafstb)-Code: concrete with recycled aggregates. In: Sustainable construction: use of recycled concrete aggregate-proceedings of the international symposium. London, UK. p. 409–18.

[32] Ministry of Housing and Urban-Rural Development of the People's Republic of China (MOHURD). JGJ 52-2006 Standard for technical requirements and test method of sand and crushed stone (or gravel) for ordinary concrete. Beijing: China Architecture & Building Press; 2006 [in Chinese].

[33] de Brito J, Barra M, Ferreira L. Influence of the pre-saturation of recycled coarse concrete aggregates on concrete properties. Mag Concr Res 2011;63:617–27.

[34] Kebaïli O, Mouret M, Arabi N, Cassagnabere F. Adverse effect of the mass substitution of natural aggregates by air-dried recycled concrete aggregates on the self-compacting ability of concrete: evidence and analysis through an example. J Clean Prod 2015;87:752–61.

[35] de Brito J, Ferreira J, Pacheco J, Soares D, Guerreiro M. Structural, material, mechanical and durability properties and behaviour of recycled aggregates concrete. J Build Eng 2016;6:1–16.

[36] Ministry of Housing and Urban-Rural Development of the People's Republic of China (MOHURD). JCJ/T 240-2011 Technical specification for application of recycled aggregate. Beijing: China Architecture & Building Press; 2011 [in Chinese].

[37] Xiao JZ, Sun YD, Falkner H. Seismic performance of frame structures with recycled aggregate concrete. Eng Struct 2006;28:1–8.

[38] Kim SW, Yun HD. Influence of recycled coarse aggregates on the bond behavior of deformed bars in concrete. Eng Struct 2013;48:133–43.

[39] Dong JF, Wang QY, Guan ZW. Structural behaviour of recycled aggregate concrete filled steel tube columns strengthened by CFRP. Eng Struct 2013;48:532–42.

[40] Behera M, Bhattacharyya SK, Minocha AK, Deoliya R, Maiti S. Recycled aggregate from C&D waste & its use in concrete-A breakthrough towards sustainability in construction sector: a review. Constr Build Mater 2014;68:501–16.

[41] China Association for Engineering Construction Standardization. CECS 28:2012 Technical specification for concrete-filled steel tubular structures. China Planning Press; 2012 [in Chinese].

[42] Matias D, de Brito J, Rosa A, Pedro D. Mechanical properties of concrete produced with recycled coarse aggregates – influence of the use of superplasticizers. Constr Build Mater 2013;44:615–21.

[43] Wang QH, Ranzi G, Wang YY, Geng Y. Long-term behaviour of simply-supported steel-bars truss slabs with recycled coarse aggregate. Constr Build Mater 2016;116:335–46.

[44] Wang YY, Wang QH, Geng Y, Ranzi G. Long-term behaviour of simply-supported composite slabs with recycled coarse aggregate. Mag Concr Res 2016. doi: http://dx.doi.org/10.1680/jmacr.16.00090.

[45] Ministry of Housing and Urban-Rural Development of the People's Republic of China (MOHURD). GB50010-2010 Code for design of concrete structures. Beijing: China Architecture & Building Press; 2011 [in Chinese].

[46] Comité Euro-International du Béton/Federation Internationale de la Pre-contrainte (CEB-FIP). CEB-FIP Model Code 1990 CEB bulletin d'Information. London: Thomas Telford; 1993.

[47] Poon CS, Shui ZH, Lam L. Effect of microstructure of ITZ on compressive strength of concrete prepared with recycled aggregates. Constr Build Mater 2004;18:461–8.

[48] Ministry of Housing and Urban-Rural Development of the People's Republic of China (MOHURD). GB/T228-2010 Metallic materials-Tensile testing-Part 1: Method of test at room temperature. Beijing: China Standard Press; 2010 [in Chinese].

[49] Han LH. Flexural behavior of concrete-filled steel tubes. J Constr Steel Res 2004;60:313–7.

[50] Padmini AK, Ramamurthy K, Mathews MS. Influence of parent concrete on the properties of recycled aggregate concrete. Constr Build Mater 2009;23:829–36.

[51] Pedro D, de Brito J, Evangelista L. Influence of the use of recycled concrete aggregates from different sources on structural concrete. Constr Build Mater 2014;71:141–51.

[52] Yu Q, Tao Z, Wu YX. Experimental behavior of high performance concrete-filled steel tubular columns. Thin Wall Struct 2008;46:362–70.

[53] Portolés JM, Romero ML, Bonet JL, Filippou FC. Experimental study of high strength concrete-filled circular tubular columns under eccentric loading. J Constr Steel Res 2011;67:623–33.